

Fuzzy Dark Matter in Relativistic Stars

Zeinab Rezaei*

*Department of Physics, School of Science, Shiraz University, Shiraz 71454, Iran.
Biruni Observatory, School of Science, Shiraz University, Shiraz 71454, Iran.*

Accepted XXX Received XXX

ABSTRACT

Fuzzy dark matter (FDM), a practical alternative to cold dark matter, can exist in compact stars. Here, applying the FDM equation of state (EoS) constrained by CMB and large-scale structure data, we calculate the structure of relativistic stars in the presence of FDM. For this aim, the EoS for the visible matter in neutron stars, quark stars, and hybrid stars from the observational data are employed. A piecewise polytropic EoS constrained by the observational data of GW170817 and the data of six low-mass X-ray binaries with thermonuclear burst or the symmetry energy of the nuclear interaction describes the neutron star matter. For quark star matter, we apply the EoSs within the Bayesian statistical approach using the mass and radius measurements of PSR J0030+0451 from NICER. Employing the two-fluid formalism, we study the structure of FDM admixed relativistic stars.

Key words: (cosmology:) dark matter, stars: interiors, cosmology: observations.

1 INTRODUCTION

Fuzzy dark matter (FDM) composed of ultralight bosonic particles with $m \sim 10^{-22} eV$ has been proposed to solve different problems such as disagreement between cold dark matter (DM) predictions and small scale observations, missing satellite problem and core-cusp problem in dwarf galaxies (Khlopov et al. 1985; Hu et al. 2000; Hui et al. 2017; Burkert 2020; Niemeyer 2020). FDM as a Bose Einstein condensate with the quantum effects at scales in the order of kpc (the de Broglie wavelength of particles) experiences quantum pressure as well as gravitational attraction. Due to the balance among the quantum pressure and the gravity, a soliton core forms near the center of FDM halo and the core structure can release the FDM particle properties (Widrow & Kaiser 1993). The behavior of FDM at large scales is not different from the cold DM, while the quantum nature of FDM influences the structure formation at small scales (Hu et al. 2000; Guth et al. 2015) and delays galaxy formation via macroscopic quantum pressure (Church et al. 2019). The wavelike nature of FDM results in the formation of granular structures in the FDM halo (Kawai et al. 2022).

Several studies have been considered to constrain the mass of FDM particles. Galaxy luminosity function at high redshifts (Schive et al. 2016; Menci et al. 2017), Lyman alpha forests (Armengaud et al. 2017; Irsic et al. 2017; Nori et al. 2019; Rogers & Peiris 2021), CMB power spectrum (Hlozek et al. 2018), radius-dependent velocity dispersion (Church et al. 2019), abundance of Milky Way

subhalos (Nadler et al. 2019, 2021), tidal streams from globular clusters (Dalal et al. 2021), galactic ultra-faint dwarf galaxies (Hayashi et al. 2021), observed displacements of star clusters and active galactic nuclei from the centers of their host galaxies (Chowdhury et al. 2021), and the observations of high-redshift lensed galaxies from CLASH survey (Kulkarni & Ostriker 2022) are some examples. Ultralight axion DM is one of the candidate for FDM (Svrcek & Witten 2006; Dave & Digal 2022). The forms of these axions have been predicted in string theory (Cicoli et al. 2022). In some investigations, the detection of axion DM has been considered (Abel et al. 2017).

FDM can influence the astrophysical objects in different scales. First galaxies are collected in a FDM cosmology and the primordial stars can form along dense DM filaments (Mocz et al. 2019). The structure of self gravitating systems containing axions (axion stars) has been investigated and the collision of axion stars with neutron stars (NSs) can release the energy of axions (Barranco et al. 2013). There may be a large number of axion stars in galaxies and their collisions with each other and with other astrophysical objects such as ordinary stars and NSs are possible (Eby et al. 2017). The attractive self-interactions of DM axions result in nongravitational growth of density fluctuations and the formation of bound objects can influence the axion density perturbations on length scales (Arvanitaki et al. 2020). Cold DM axions may be converted into photons in the NS magnetosphere (Huang et al. 2018; Foster et al. 2020; Battye et al. 2021). Axion DM can be detected via the narrow radio lines radiated by the NSs (Huang et al. 2018; Hook et al. 2018;

* E-mail: zrezaei@shirazu.ac.ir

Safdi et al. 2019; Foster et al. 2020). Pulsar timing array experiment has been suggested to detect the FDM signals (Khmelnitsky & Rubakov 2014; Porayko & Postnov 2014; Martino et al. 2017; Porayko et al. 2018; Kato & Soda 2020; Nomura et al. 2020). FDM affects the dynamics of binary systems (Nacir & Urban 2018; Armaleo et al. 2020). Variations of the orbital parameters of binary systems induced by the perturbations of FDM have been studied (Blas et al. 2020).

Recently, DM in different compact objects such as NSs and quark stars (QSSs) has been one of the interesting subjects in astrophysics. NSs can constrain the asymmetric DM (Garani et al. 2019; Ivanytskyi et al. 2020). Low-mass NSs can be formed from the accretion-induced collapse of DM admixed white dwarfs (Leung et al. 2019). Spectroscopy measurements of NSs have been employed to detect DM (Camargo et al. 2019; Maity & Queiroz 2021). NSs admixed with DM and the constraints on DM properties from the observation of GW170817 (Quddus et al. 2020) have been explored. DM particles can be captured by NSs and this leads to the NSs thermalization (Bell et al. 2019; Acevedo et al. 2020; Keung et al. 2020; Bell et al. 2020; Garani et al. 2021; Bell et al. 2021a,b; Anzuini et al. 2021; Kumar et al. 2022). DM interactions with muons (Garani & Heeck 2019), DM Admixed NSs with the DM-nucleons interactions via Higgs portal (Bhat & Paul 2020), and self-interacting bosonic DM (Rafiei Karkevandi et al. 2022) have been considered. DM affects the nuclear matter parameters and the equations of state (EoSs) of nucleonic-matter (Das et al. 2020) and the curvatures of the NS (Das et al. 2021). By modeling a massive NS with DM particles, the secondary component of GW190814 has been constrained (Das et al. 2021). The possibility of the fact that GW190814 is a bosonic DM admixed compact star has been studied (Lee et al. 2021). Mass radius relation and second Love number of stars containing ordinary matter and non-self annihilating fermionic DM have been calculated (Dengler et al. 2022). The transmutation of NSs admixed with DM and gravitational collapse in the star centers result in the formation of black holes with masses $M \approx 1M_{\odot}$ (Garani et al. 2022). Dynamical evolution of DM admixed NSs with fermionic DM has been investigated (Gleason et al. 2022).

Self-annihilating neutralino WIMP DM may accrete into NSs and compact objects with long-lived lumps of strange quark matter form (Perez-Garcia et al. 2010). The regions of stability for compact stars containing massless quark matter and fermionic DM have been calculated (Mukhopadhyay & Schaffner-Bielich 2016). The observation of strange QSSs could set constraints on the scattering cross sections of light quarks and non-interacting scalar DM (Zheng & Chen 2016). The structure of strange stars admixed with self-interacting bosonic DM has been considered (Panotopoulos & Lopes 2017a,b; Lopes & Panotopoulos 2018). The observations of strange stars in GW170817 confirmed that these stars have a mirror DM core (Yang et al. 2021). According to the above discussions, one can easily conclude that the FDM can have important effects on relativistic stars. In this paper, we study the structure of NSs, QSSs, and hybrid stars in the presence of FDM.

2 FUZZY DARK MATTER CONSTRAINED BY THE OBSERVATIONAL DATA

In this study, we employ a constrained FDM model with a quartic self-interaction (Cembranos et al. 2018). For this aim, a scalar field ϕ , with Lagrangian

$$\mathcal{L} = \frac{1}{2}g^{\mu\nu}\partial_{\mu}\phi\partial_{\nu}\phi - V(\phi), \quad (1)$$

are considered. The potential has the form

$$V(\phi) = \frac{1}{2}m^2\phi^2 + \frac{1}{4}\lambda\phi^4, \quad (2)$$

in which m denotes the mass term and λ shows the strength of quartic self-interactions. Assuming a homogeneous and isotropic universe with a flat Robertson-Walker metric, anharmonic corrections to the mass term lead to the EoS for the scalar field with pressure P and density ρ ,

$$w = \frac{P}{\rho}, \quad (3)$$

with

$$w = \frac{\frac{3\lambda}{8m^4}\rho}{1 + \frac{9\lambda}{8m^4}\rho}. \quad (4)$$

Applying CMB (Ade et al. 2016) and large-scale structure (LSS) (Parkinson et al. 2012) data, the parameters of this model have been constrained (Cembranos et al. 2018). The constraint for the mass is $m \geq 10^{-24} eV$ and for allowed masses, the constraint on λ is as follows,

$$\log_{10}\lambda < -91.86 + 4\log_{10}(\frac{m}{10^{-22}eV}). \quad (5)$$

Here, to describe FDM, we apply the values $m = 10^{-24} eV$ for the mass and $\lambda = 10^{-100}$ for the self-interactions of FDM. In Figure. 1, we have presented the EoS of FDM constraint with the observational data.

3 TWO-FLUID FORMALISM FOR FUZZY DARK MATTER ADMIXED STARS

Starting with two-fluid formalism (Sandin & Ciarcelluti 2009; Ciarcelluti & Sandin 2011), we apply one static and spherically symmetric spacetime described by the line element,

$$d\tau^2 = e^{2\nu(r)}dt^2 - e^{2\lambda(r)}dr^2 - r^2(d\theta^2 + \sin^2\theta d\phi^2), \quad (6)$$

and the energy momentum tensor of a perfect fluid,

$$T^{\mu\nu} = -pg^{\mu\nu} + (p + \varepsilon)u^{\mu}u^{\nu}. \quad (7)$$

In the expression $T^{\mu\nu}$, p and ε are the total pressure and total energy density, respectively, which are the results of both visible (V) and dark (D) sectors,

$$p(r) = p_V(r) + p_D(r), \quad (8)$$

$$\varepsilon(r) = \varepsilon_V(r) + \varepsilon_D(r). \quad (9)$$

In Eq. (8), p_V stands for the EoS of visible matter in compact stars, while p_D presents the FDM EoS given by Eq. (3). Considering the above profiles, the Einstein field equations result in (Sandin & Ciarcelluti 2009; Ciarcelluti & Sandin 2011)

$$e^{-2\lambda(r)} = 1 - \frac{2M(r)}{r}, \quad (10)$$

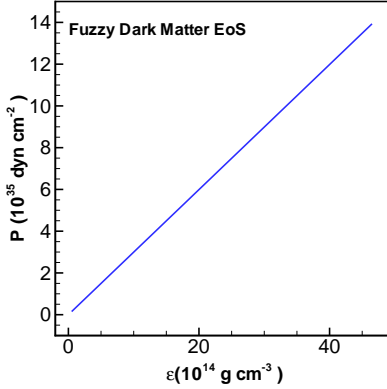


Figure 1. Fuzzy dark matter EoS with the parameters $m = 10^{-24} \text{ eV}$ and $\lambda = 10^{-100}$ from the observational data.

$$\frac{d\nu}{dr} = \frac{M(r) + 4\pi r^3 p(r)}{r[r - 2M(r)]}, \quad (11)$$

$$\frac{dp_V}{dr} = -[p_V(r) + \varepsilon_V(r)] \frac{d\nu}{dr}, \quad (12)$$

$$\frac{dp_D}{dr} = -[p_D(r) + \varepsilon_D(r)] \frac{d\nu}{dr}. \quad (13)$$

Here, $M(r) = \int_0^r dr 4\pi r^2 \varepsilon(r)$ denotes the total mass inside a sphere with radius r and we specify the visible matter sphere and DM sphere with the conditions $p_V(R_V) = 0$ and $p_D(R_D) = 0$, respectively. In this work, we assume that the densities of visible matter and dark matter are the same in the center of the star.

For the stars in the binaries, the tidal forces lead to induce the tidal deformabilities in the stars (Hinderer et al. 2010). The traceless quadrupole moment tensor of the star Q_{ij} is related to the tidal field tensor E_{ij} by

$$Q_{ij} = -\frac{2}{3}k_2 R_V^5 E_{ij} = -\lambda E_{ij}, \quad (14)$$

in which $\lambda = \frac{2}{3}k_2 R_V^5$ denotes the tidal deformability. Besides, the tidal Love number k_2 is as follows (Hinderer 2008),

$$\begin{aligned} k_2 &= \frac{8\beta^5}{5}(1-2\beta)^2[2-y_R+(y_R-1)2\beta] \\ &\times [2\beta(6-3y_R+3\beta(5y_R-8)) \\ &+ 4\beta^3(13-11y_R+\beta(3y_R-2)+2\beta^2(1+y_R)) \\ &+ 3(1-2\beta)^2[2-y_R+2\beta(y_R-1)]\ln(1-2\beta)]^{-1}. \end{aligned} \quad (15)$$

and $\beta = M/R$ presents the compactness of the star. Furthermore, solving the following differential equation leads to the value of $y_R = y(r = R_V)$,

$$r \frac{dy(r)}{dr} + y^2(r) + y(r)F(r) + r^2Q(r) = 0. \quad (16)$$

The functions $F(r)$ and $Q(r)$ are given by,

$$F(r) = [1 - 4\pi r^2(\varepsilon(r) - p(r))] \left(1 - \frac{2M(r)}{r}\right)^{-1}, \quad (17)$$

and

$$r^2Q(r) = 4\pi r^2[5\varepsilon(r) + 9p(r) + \frac{\varepsilon(r) + p(r)}{\partial p(r)/\partial \varepsilon(r)}]$$

$$\begin{aligned} &\times \left(1 - \frac{2M(r)}{r}\right)^{-1} - 6\left(1 - \frac{2M(r)}{r}\right)^{-1} \\ &- \frac{4M^2(r)}{r^2} \left(1 + \frac{4\pi r^3 p(r)}{M(r)}\right)^2 \left(1 - \frac{2M(r)}{r}\right)^{-2}, \end{aligned} \quad (18)$$

We solve Eq. (16) along Eqs. (10)-(13) with the initial condition $y(0) = 2$. In addition, the dimensionless tidal deformability is defined by

$$\Lambda = \frac{2}{3}k_2 \frac{R_V^5}{M^5}. \quad (19)$$

In the case of quark star which is self bound, the discontinuity of the energy density at the surface of star should be considered. In the present study, we apply the boundary treatment on the stellar surface to join the interior solution with the exterior one as in Refs. (Damour & Nagar 2009; Postnikov et al. 2010; Zhou et al. 2018),

$$y_R^{ext} = y_R^{int} - \frac{\varepsilon_s}{M/4\pi R_V^3}, \quad (20)$$

in which ε_s is the energy density at the surface of star.

4 FUZZY DARK MATTER ADMIXED NEUTRON STAR

In order to quantify the visible matter in NSs, we utilize the EoS of dense NS matter in the form of a piecewise polytropic expansion which is constrained by the observational data of GW170817 and the data of six low-mass X-ray binaries (LMXB) with thermonuclear burst or the symmetry energy of the nuclear interaction (Jiang et al. 2019). The EoS with the expression $P = K\rho^\Gamma$ is parameterized with four pressure parameters $\{\hat{p}_1, \hat{p}_2, \hat{p}_3, \hat{p}_4\}$ at the corresponding densities of $\{1, 1.85, 3.7, 7.4\}\rho_{sat}$ in which the saturation density has the value $\rho_{sat} = 2.7 \times 10^{14} \text{ g cm}^{-3}$ (Ozel & Psaltis 2009). The joint analysis confirms that the constraint on \hat{p}_1 mainly is the result of nuclear constraints, the constraint on \hat{p}_2 is predominantly determined by the gravitational wave data and the LMXB sources with thermonuclear bursts, the constraint on \hat{p}_3 heavily comes from the LMXB source data and the current bounds of M_{TOV} , and the range of \hat{p}_4 is narrowed down by LMXB sources with thermonuclear burst.

Piecewise polytropic EoS of NS matter and the mass radius relation for both NS and NS admixed with FDM

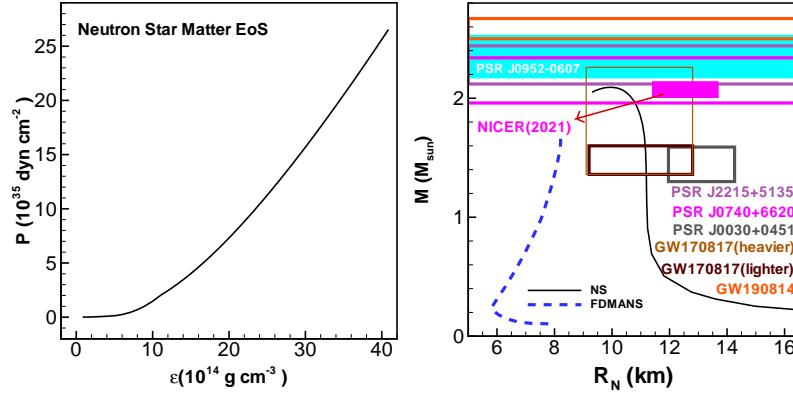


Figure 2. Left: EoS of dense neutron star matter constrained by the observational data and Right: Mass radius relation in the cases of neutron star (NS) and FDM admixed neutron star (FDMANS). Observational constraints on the NS radii and masses from the pulsars and the gravitational wave data are also presented. These constraints are related to NICER observations for PSR J0952-0607 (Romani et al. 2022), PSR J2215+5135 (Linares et al. 2018), PSR J0740+6620 (Cromartie et al. 2020; Fonseca et al. 2021; Miller et al. 2021; Riley et al. 2021), PSR J0030+0451 (Miller et al. 2019), and the merger events GW170817 (Abbott et al. 2017, 2018) and GW190814 (Abbott et al. 2020).

are given in Figure. 2. For the FDM admixed neutron star (FDMANS), we have considered the total mass versus the visible radius, i.e. the radius of sphere containing NS matter. FDM leads to stars with lower masses. The radius of FDMANSs is smaller than the radius of NSs with the same mass. Therefore, FDM results in more compact stars. For most FDMANSs, the larger stars are more massive, in contrary with NSs. The interaction between FDM and NS matter leads to the self-bound FDMANSs a behavior different from the normal NSs which are gravitationally bound. We have also shown the constraints on the mass radius relation obtained from the pulsars and the gravitational wave data with different colour bars. NICER observations for PSR J0952-0607 (Romani et al. 2022), PSR J2215+5135 (Linares et al. 2018), PSR J0740+6620 (Cromartie et al. 2020; Fonseca et al. 2021; Miller et al. 2021; Riley et al. 2021), PSR J0030+0451 (Miller et al. 2019), and the merger events GW170817 (Abbott et al. 2017, 2018) and GW190814 (Abbott et al. 2020) give these constraints. Both NSs and FDMANSs satisfy the constraints from the recent observational data. The presented observations confirm that the maximum mass of FDMANSs is lower than the value $\sim 2.0M_{\odot}$. FDM leads to stars with lower maximum mass than all the observational data shown in this figure.

Figure. 3 explains the behavior of visible and dark sectors in FDMANSs. In very low mass stars, the mass of two sectors is not sensitive to the size of spheres. However, for other FDMANSs, the mass of visible and dark spheres grows by increasing the radius. The results confirm that for dark sphere, this behavior is not valid for all stars and in large dark spheres, the mass decreases as the radius grows. Figure. 3 verifies that in smaller FDMANSs, the mass of dark sphere is higher than the NS matter sphere. However, in larger FDMANSs, the mass of visible sector is dominant. This opposite behavior for visible and dark sectors in FDMANS is due to the different EoSs of two sectors.

In Figure. 4, we have presented the tidal Love number k_2 , the value y_R , and the dimensionless tidal deformability Λ in the cases of NSs and FDMANSs. Except for the low mass stars, the tidal Love number decreases due to presence of the FDM in the stars. Besides, the star mass corresponding to the maximum value of the tidal Love number is lower when the FDM is considered in the stars. However, the value y_R is higher in FDMANSs compared to NSs for most cases. Our calculations confirm that the dimensionless tidal deformability decreases with the star mass for both NSs and FDMANSs. The FDM leads to a considerable reduction of the dimensionless tidal deformability. This decrease is more significant in low mass stars. Moreover, we have shown the upper limits on dimensionless tidal deformability $\Lambda_{1.4} = 190^{+390}_{-120}$ for GW170817 (Abbott et al. 2018) and $\Lambda_{1.4} = 616^{+273}_{-158}$ for GW190814 (Abbott et al. 2020) obtained by LIGO and Virgo Collaborations. In NSs, the dimensionless tidal deformability is in the range $70 \leq \Lambda_{1.4} \leq 580$ related to GW170817. This is while the parameter Λ for NSs is lower than $\Lambda_{1.4} = 616^{+273}_{-158}$ related to GW190814. Considering the FDMANSs, both upper limits from GW170817 and GW190814 are larger than the dimensionless tidal deformability.

5 FUZZY DARK MATTER ADMIXED QUARK STAR

In this work, we apply three EoSs of QSSs within the Bayesian statistical approach using the mass and radius measurements of PSR J0030+0451 from NICER (Li et al. 2021). These self-bound strange quark matter EoSs are based on the bag models in which the finite quark mass and superfluidity are also considered. Our system describing the strange quark matter is a mixture of the massless u, d quarks and electrons, as well as s quarks of finite mass m_s (Haensel et al. 1986).

In the first model, i.e. normal quark matter, the grand canonical potential per unit volume in the bag model is ex-

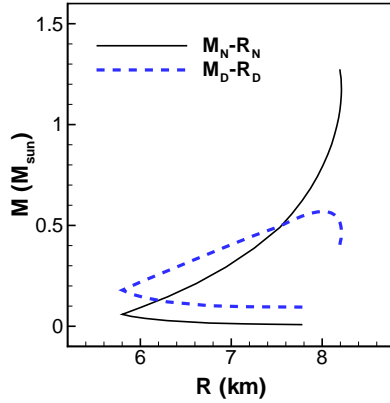


Figure 3. Mass radius relation for two sectors of neutron star matter ($M_N - R_N$) and dark matter ($M_D - R_D$) in FDMANS.

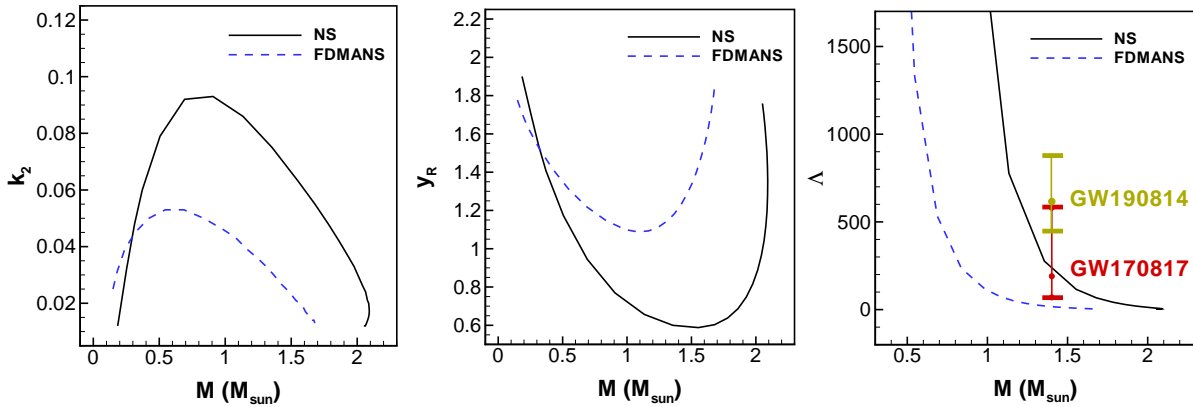


Figure 4. Tidal Love number k_2 , the value y_R , and the dimensionless tidal deformability Λ versus the mass for NS and FDMANS. The constraints from GW170817 and GW190814 data (LIGO and Virgo Collaborations) for neutron star of mass $M = 1.4M_\odot$ are also given. These upper limits on dimensionless tidal deformability are $\Lambda_{1.4} = 190^{+390}_{-120}$ for GW170817 (Abbott et al. 2018) and $\Lambda_{1.4} = 616^{+273}_{-158}$ for GW190814 (Abbott et al. 2020).

pressed by,

$$\Omega_{Normal} = \sum_{i=u,d,s,e} \Omega_i^0 + \frac{3(1-a_4)}{4\pi^2} \mu^4 + B_{eff}. \quad (21)$$

Here, Ω_i^0 denotes the grand canonical potential for particle type i as the ideal Fermi gas (Farhi & Jaffe 1984) and $\mu = (\mu_u + \mu_d + \mu_s)/3$ presents the average quark chemical potential. In addition, B_{eff} determines the contributions from the quantum chromodynamics (QCD) vacuum, and a_4 shows the perturbative QCD contribution from one-gluon exchange for gluon interaction. Besides, the number density of each part of strange quark matter is related to the chemical potential $\mu_i (i = u, d, s, e)$ by,

$$n_i = -\frac{\partial \Omega}{\partial \mu_i}. \quad (22)$$

The conditions for the quark matter at the equilibrium state

are given by the weak interactions,

$$\mu_d = \mu_u + \mu_e, \quad (23)$$

$$\mu_d = \mu_s. \quad (24)$$

The condition of charge neutrality is also considered,

$$\frac{2}{3}n_u = \frac{1}{3}[n_d + n_s] + n_e. \quad (25)$$

For normal quark matter, the pressure of quark matter at each value of μ is calculated by,

$$P_{Normal} = -\Omega_{Normal}, \quad (26)$$

and the energy density of quark matter is as follows,

$$\varepsilon_{Normal} = \Omega_{Normal} + \sum_{i=u,d,s,e} \mu_i n_i. \quad (27)$$

In the two-parameter model $Normal(B_{eff}; a_4)$, the strange quark mass is fixed as $m_s = 100$ MeV and the two pa-

rameters ($B_{eff}; a_4$) are determined from the joint MSP J0740+6620 and PSR J0030+0451 analysis (Li et al. 2021).

The second model describing the superfluid quark matter is Color-Flavor Locked (CFL) in which an additional term related to the pairing energy is added to the grand canonical potential (Li et al. 2021),

$$\Omega_{CFL} = \Omega_{Normal} + \frac{3m_s^4 - 48\Delta^2\mu^2}{16\pi^2}. \quad (28)$$

In the three-parameter model $CFL(B_{eff}; a_4; \Delta)$, as Normal model, the strange quark mass is $m_s = 100$ MeV and the three parameters ($B_{eff}; a_4; \Delta$) are constrained by the observational data (Li et al. 2021). The third model is four-parameter model $CFLm(B_{eff}; a_4; \Delta; m_s)$ in which the strange quark mass m_s of the CFL superfluid quark matter is also constrained by the observational data (Li et al. 2021).

Figure. 5 presents the three models for the EoS of strange star matter considered in this work. In CFL and CFLm models, the EoS is stiffer than the EoS in Normal model. CFLm model also leads to EoS which is stiffer than the EoS in CFL model. The mass radius relation for QSs and FDM admixed QSs (FDMAQSs) is given in Figure. 6. In each model for quark matter, the maximum mass of FDMAQSs reaches the value lower than the one for QSs. FDM affects the star so that the FDMAQSs are smaller than QSs with the same mass. Therefore, the FDM leads to more compact stars, like the effect in NSs. This result is in agreement with the one obtained in (Yang et al. 2021). QSs fulfill both the maximum mass and the mass radius constraints from the presented observational data. In addition, the maximum mass of FDMAQSs is lower than the value related to the maximum mass constraints.

Figures. 7 shows the mass radius relation for visible and dark sectors in FDMAQSs. In three models, both visible and dark sectors represent a self-bound behavior like QS and FDMAQS. For two spheres with smaller sizes, the mass of sphere is not sensitive to the size. For most FDMAQSs, the contribution of two sectors in the mass of stars is the same. This is while in massive stars, the mass of visible sphere is higher than the dark one.

The tidal Love number k_2 , the value y_R , and the dimensionless tidal deformability Λ for QSs and FDMAQSs are given in Figure. 8. In most FDMAQSs, the tidal Love number takes higher values compared to the one in QSs with the same mass. This is while in massive FDMAQSs, FDM leads to the reduction of tidal Love number. Generally, FDMAQSs can experience larger values of the tidal Love number. Figure. 8 also indicates that for both QSs and FDMAQSs y_R increases as the mass grows. y_R for FDMAQSs is larger than for QSs. Our calculations confirm that FDM in QSs results in a considerable decrease of the dimensionless tidal deformability similar to the behavior in NSs. Besides, for both QSs and FDMAQSs, the dimensionless tidal deformability is lower than the upper limits from GW170817 and GW190814.

6 FUZZY DARK MATTER ADMIXED HYBRID STAR

For this study, we suppose that the hybrid star is composed of a quark phase and a hadronic phase within a model like the one considered in (Pereira et al. 2021). In our model, these two parts are split by a sharp phase-transition surface without a mixed phase and the density at the phase-splitting surface can be discontinuous (Pereira et al. 2020).

For the quark phase, we apply three EoSs, i.e. Normal, CFL, and CFLm models. Furthermore, to describe the hadronic phase, the EoS of dense NS matter based on the observational data which considered in section 4 is applied. The density jump at the surface of quark-hadronic phase transition is taken as a free parameter. By defining the parameter,

$$\eta \equiv \frac{\epsilon_q}{\epsilon_h} - 1, \quad (29)$$

in which ϵ_q shows the density at the top of the quark phase and ϵ_h denotes the density at the bottom of the hadronic phase, we quantify the density jump. According to $p_q = p_h$ at the quark-hadronic phase transition interface, ϵ_q or ϵ_h and the phase transition pressure are determined.

In Figure. 9, we have presented the mass radius relation for hybrid star and FDM admixed hybrid star (FDMAHS) in two cases $\eta = 0$ and $\eta = 0.8$. FDM affects the mass of hybrid stars in a way that the maximum mass decreases. Similar to other compact objects, the FDMAHSs are smaller in size compared to hybrid stars. The FDM results in more compact stars. Similar to QSs, HSs also satisfy both the maximum mass and the mass radius constraints. Moreover, our results verify that FDMAHSs fulfill the maximum mass constraint.

Figure. 10 gives the mass radius relations of visible and dark sectors in FDMAHSs. The mass of sphere containing visible matter increases as the size grows. In all models, the spheres are self-bound with different contributions of visible and dark matter in low and massive stars. In discontinuous model, the range of the size of radius is higher than the one in continuous model. The low values of the mass of each visible and dark sectors show the contribution of these parts in the total mass of FDMAHSs. Besides, Figure. 10 verifies that FDM results in the contraction of the FDMAHSs and smaller radius of stars.

For HSs and FDMAHSs, we have shown the tidal Love number k_2 , the value y_R , and the dimensionless tidal deformability Λ in Figure. 11. Except in low mass FDMAHSs, the tidal Love number of FDMAHSs is smaller than the one in HSs. Besides, considering HSs, the tidal Love number is larger in discontinuous model. However, in FDMAHSs, the tidal Love number is almost the same in continuous and discontinuous models. In addition, considering FDMAHSs, the value y_R is smaller than the one in HSs. The discontinuous model gives lower values for y_R . Our calculations confirm that FDM considerably reduces the dimensionless tidal deformability of FDMAHSs like the one in FDMANSs and FDMAQSs. The dimensionless tidal deformability is higher in the discontinuous model compared to the continuous one. This enhancement is more significant in the low mass stars. Our calculations verify that for both HSs and FDMAHSs, the dimensionless tidal deformability is lower than the upper limits from GW170817 and GW190814.

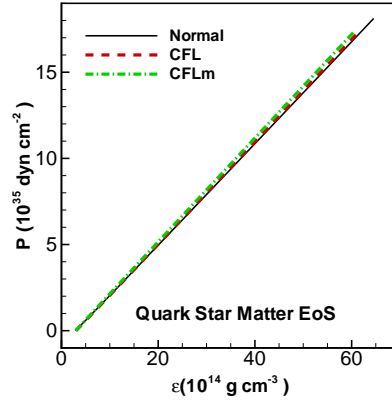


Figure 5. Three EoSs of quark star matter based on the bag models constraint with the NICER data.

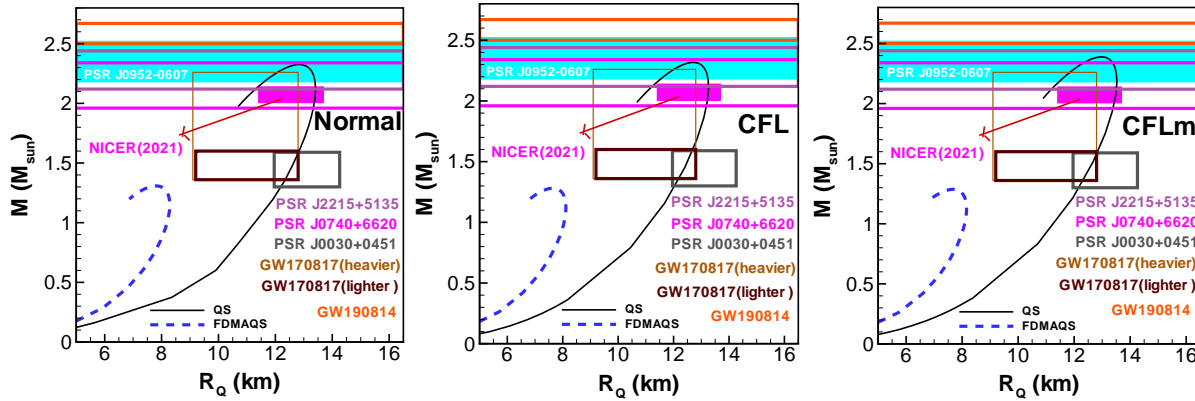


Figure 6. Mass radius relation for quark star (QS) and FDM admixed quark star (FDMAQS) in three models for the EoS of quark star matter. Observational constraints are the same as Figure. 2.

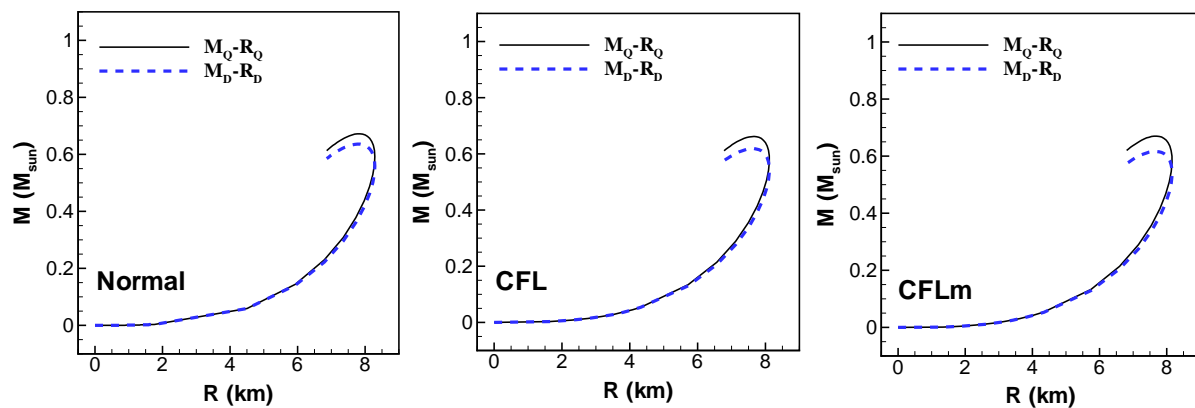


Figure 7. Mass radius relation for two sectors of quark star matter ($M_Q - R_Q$) and dark matter ($M_D - R_D$) in FDMAQS.

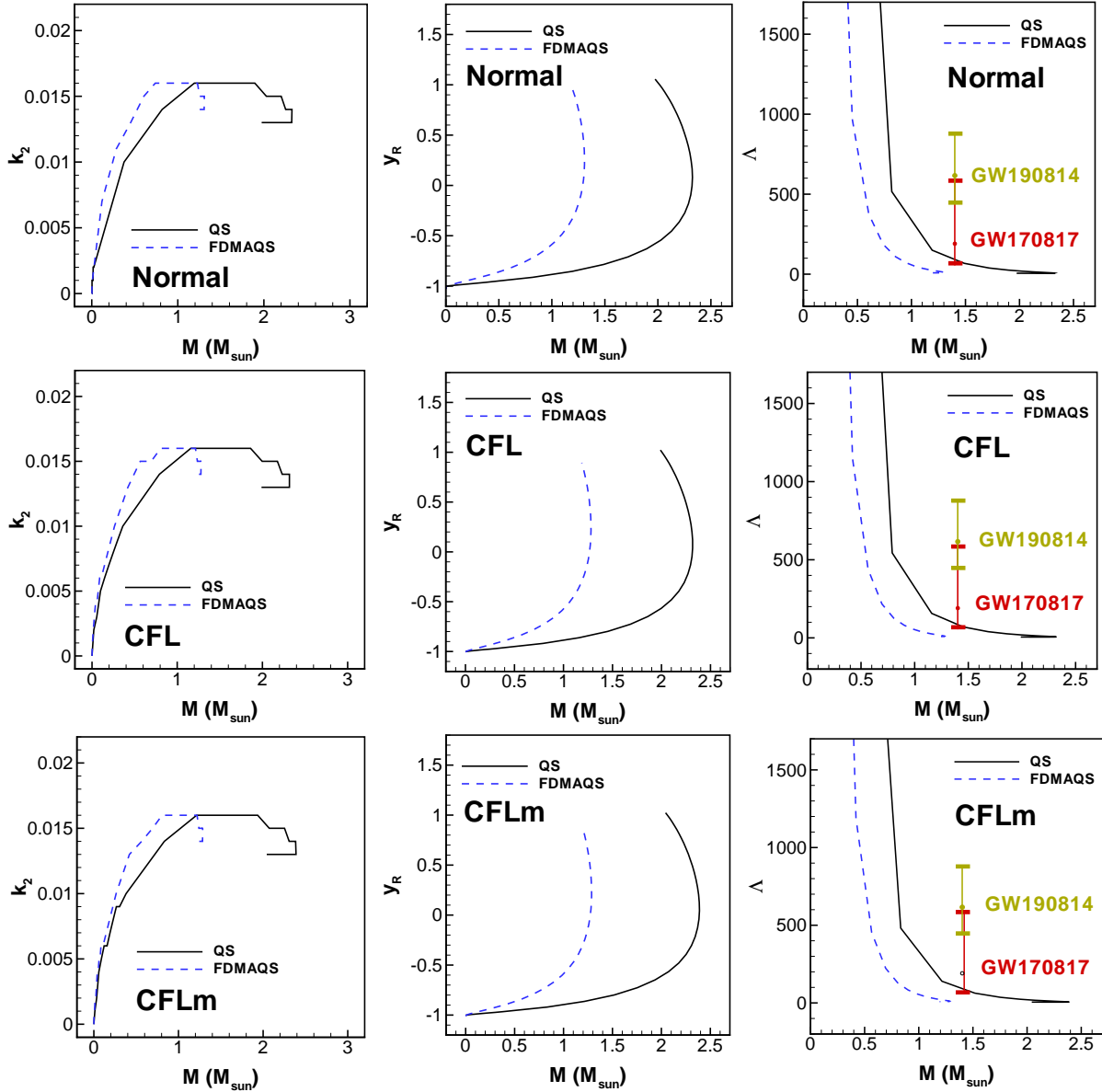


Figure 8. Tidal Love number k_2 , the value y_R , and the dimensionless tidal deformability Λ versus the mass in the cases of QS and FDMAQS in three models for the EoS of quark star matter. Observational constraints are the same as Figure 4.

7 SUMMARY AND CONCLUSIONS

In the relativistic two-fluid formalism, we have explored the effects of fuzzy dark matter (FDM) on the compact stars. The equations of state for FDM as well as the visible matter in stars which have been used are based on the observational data. Our results verify that in FDM admixed neutron stars, FDM leads to neutron stars with lower masses. Moreover, FDM makes more compact neutron stars. In FDM admixed neutron stars, the mass of visible and dark spheres grows as the radius increases. Besides, the mass of visible and dark spheres depends on the size of the stars. FDM admixed quark stars are smaller than quark stars without FDM with the same mass and therefore they are more compact, like the

phenomena in neutron stars. FDM admixed hybrid stars are also more compact in comparison with hybrid stars with no FDM. Furthermore, FDM in compact stars leads to a significant change in the dimensionless tidal deformability of stars.

ACKNOWLEDGEMENTS

The author wishes to thank the Shiraz University Research Council.

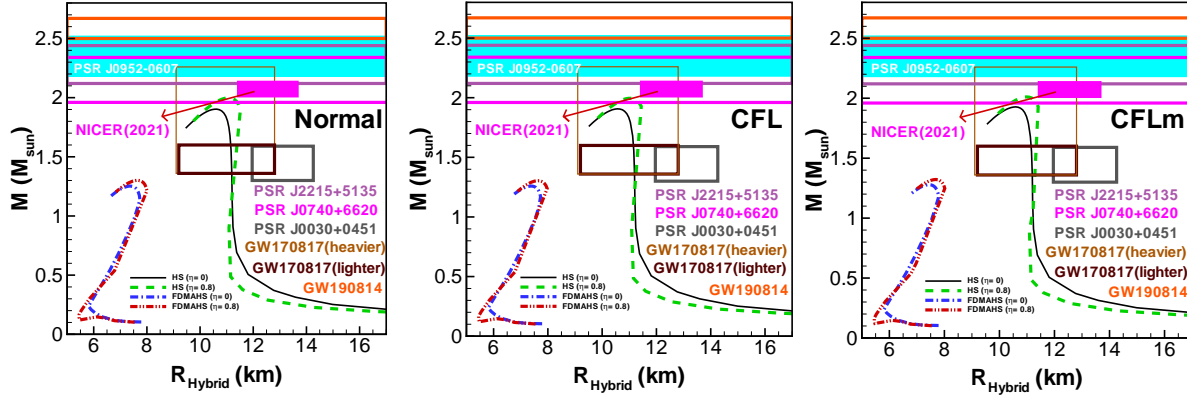


Figure 9. Mass radius relation for hybrid star (HS) and FDM admixed hybrid star (FDMAHS) for two cases $\eta = 0$ and $\eta = 0.8$ in different models of quark matter EoS for the quark phase. Observational constraints are the same as Figure. 2

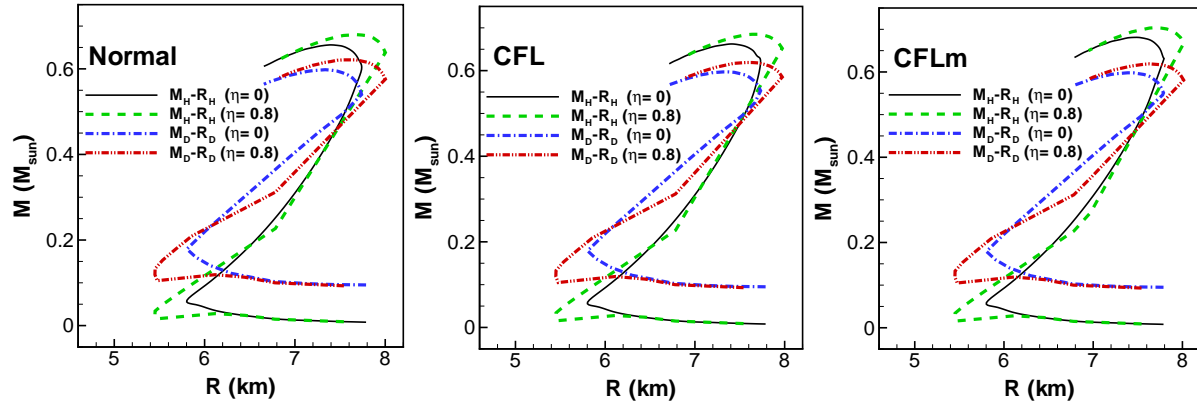


Figure 10. Mass radius relation for two sectors of hadronic matter ($M_H - R_H$) and dark matter ($M_D - R_D$) in FDMAHS for two cases $\eta = 0$ and $\eta = 0.8$ in different models of quark matter EoS for the quark phase.

DATA AVAILABILITY

All data are given either in this paper or in the references.

REFERENCES

- Abbott B. P., et al., 2017, PhRvL, 119, 161101. doi:10.1103/PhysRevLett.119.161101
- Abbott B. P., et al., 2018, PhRvL, 121, 161101. doi:10.1103/PhysRevLett.121.161101
- Abbott R., et al., 2020, ApJL, 896, L44. doi:10.3847/2041-8213/ab960f
- Abel C., et al., 2017, PhRvX, 7, 041034. doi:10.1103/PhysRevX.7.041034
- Acevedo J. F., Bramante J., Leane R. K., Raj N., 2020, JCAP, 03, 038. doi:10.1088/1475-7516/2020/03/038
- Ade P. A. R., et al., 2016, A and A, 594, A13. doi:10.1051/0004-6361/201525830
- Anzuini F., et al., 2021, JCAP, 11, 056. doi:10.1088/1475-7516/2021/11/056
- Armaeleo J. M., Nacir D. L., Urban F. R., 2020, JCAP, 01, 053. doi:10.1088/1475-7516/2020/01/053
- Armengaud E., Palanque-Delabrouille N., Yèche C., Marsh D. J. E., Baur J., 2017, MNRAS, 471, 4606. doi:10.1093/mnras/stx1870
- Arvanitaki A., Dimopoulos S., Galanis M., Lehner L., Thompson J. O., Tilburg K. V., 2020, PhRvD, 101, 083014. doi:10.1103/PhysRevD.101.083014
- Barranco J., Monteverde A. C., Delepine D., 2013, PhRvD, 87, 103011. doi:10.1103/PhysRevD.87.103011
- Battye R. A., Garbrecht B., McDonald J., Srinivasan S., 2021, JHEP, 2021, 105. doi:10.1007/JHEP09(2021)105
- Bell N. F., Busoni G., Robles S., 2019, JCAP, 06, 054. doi:10.1088/1475-7516/2019/06/054
- Bell N. F., Busoni G., Robles S., Virgato M., 2020, JCAP, 09, 028. doi:10.1088/1475-7516/2020/09/028
- Bell N. F., Busoni G., Robles S., Virgato M., 2021, JCAP, 03, 086. doi:10.1088/1475-7516/2021/03/086
- Bell N. F., et al., 2021, PhRvL, 127, 111803.

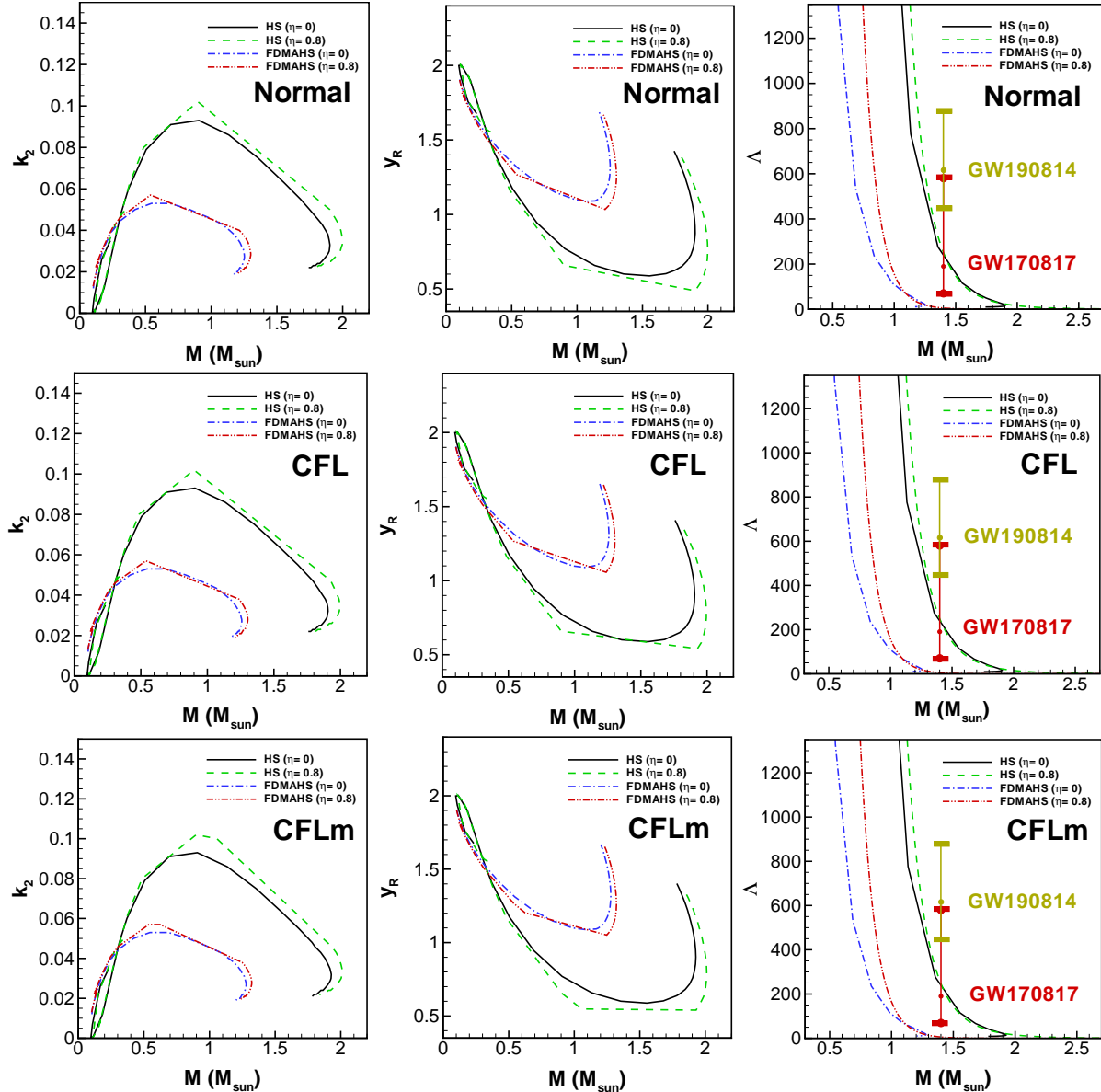


Figure 11. Tidal Love number k_2 , the value y_R , and the dimensionless tidal deformability Λ versus the mass in HS and FDMAHS for two cases $\eta = 0$ and $\eta = 0.8$ in different models of quark matter EoS for the quark phase. Observational constraints are the same as Figure 4.

- doi:10.1103/PhysRevLett.127.1111803
 Bhat S. A., Paul A., 2020, EPJC, 80, 544.
 doi:10.1140/epjc/s10052-020-8072-x
 Blas D., Nacir D. L., Sibiryakov S., 2020, PhRvD, 101, 063016. doi:10.1103/PhysRevD.101.063016
 Burkert A., 2020, ApJ, 904, 161. doi:10.3847/1538-4357/abb242
 Camargo D. A., Queiroz F. S., Sturani R., 2019, JCAP, 09, 051. doi:10.1088/1475-7516/2019/09/051
 Cembranos J. A. R., Maroto A. L., Nunez Jareno S. J., Villarrubia-Rojo H., 2018, JHEP, 2018, 73. doi:10.1007/JHEP08(2018)073

- Chowdhury D. D., et al., 2021, ApJ, 916, 27. doi:10.3847/1538-4357/ac043f
 Church B. V., Mocz P., Ostriker J. P., 2019, MNRAS, 485, 2861. doi:10.1093/mnras/stz534
 Ciarcelluti P., Sandin F., 2011, Phys. Lett. B, 695, 19. doi:10.1016/j.physletb.2010.11.021
 Cicoli M., et al., 2022, JHEP, 2022, 107. doi:10.1007/JHEP05(2022)107
 Cromartie H. T., et al., 2020, NatAs, 4, 72. doi:10.1038/s41550-019-0880-2
 Dalal N., Bovy J., Hui L., Li X., 2021, JCAP, 03, 076. doi:10.1088/1475-7516/2021/03/076

- Damour T., Nagar A., 2009, *PhRvD*, 80, 084035. doi:10.1103/PhysRevD.80.084035
- Das H. C., et al., 2020, *MNRAS*, 495, 4893. doi:10.1093/mnras/staa1435
- Das H. C., Kumar A., Kumar B., Biswal S. K., Patra S. K., 2021, *JCAP*, 01, 007. doi:10.1088/1475-7516/2021/01/007
- Das H. C., Kumar A., Patra S. K., 2021, *PhRvD*, 104, 063028. doi:10.1103/PhysRevD.104.063028
- Dave S. S., Digal S., 2022, *PhRvD*, 105, 024039. doi:10.1103/PhysRevD.105.024039
- Dengler Y., Schaffner-Bielich J., Tolos L., 2022, *PhRvD*, 105, 043013. doi:10.1103/PhysRevD.105.043013
- Eby J., et al., 2017, *JHEP*, 2017, 99. doi:10.1007/JHEP04(2017)099
- Farhi E., Jaffe R. L., 1984, *PhRvD*, 30, 2379. doi:10.1103/PhysRevD.30.2379
- Fonseca E., Cromartie H. T., Pennucci T. T., et al., 2021, *ApJL*, 915, L12. doi:10.3847/2041-8213/ac03b8
- Foster J. W., et al., 2020, *PhRvL*, 125, 171301. doi:10.1103/PhysRevLett.125.171301
- Garani R., Genolini Y., Hambye T., 2019, *JCAP*, 05, 035. doi:10.1088/1475-7516/2019/05/035
- Garani R., Heeck J., 2019, *PhRvD*, 100, 035039. doi:10.1103/PhysRevD.100.035039
- Garani R., Gupta A., Raj N., 2021, *PhRvD*, 103, 043019. doi:10.1103/PhysRevD.103.043019
- Garani R., Levkov D., Tinyakov P., 2022, *PhRvD*, 105, 063019. doi:10.1103/PhysRevD.105.063019
- Gleason T., Brown B., Kain B., 2022, *PhRvD*, 105, 023010. doi:10.1103/PhysRevD.105.023010
- Guth A. H., Hertzberg M. P., Prescod-Weinstein C., 2015, *PhRvD*, 92, 103513. doi:10.1103/PhysRevD.92.103513
- Haensel P., Zdunik J. L., Schaefer R., 1986, *A and A*, 160, 121. doi:1986A and A...160..121H
- Hayashi K., Ferreira E. G. M., Chan H. Y. J., 2021, *ApJL*, 912, L3. doi:10.3847/2041-8213/abf501
- Hinderer T., Lackey B. D., Lang R. N., Read J. S., 2010, *PhRvD*, 81, 123016. doi:10.1103/PhysRevD.81.123016
- Hinderer T., 2008, *ApJ*, 677, 1216. doi:10.1086/533487
- Hlozek R., Marsh D. J. E., Grin D., 2018, *MNRAS*, 476, 3063. doi:10.1093/mnras/sty271
- Hook A., Kahn Y., Safdi B. R., Sun Z., 2018, *PhRvL*, 121, 241102. doi:10.1103/PhysRevLett.121.241102
- Hu W., Barkana R., Gruzinov A., 2000, *PhRvL*, 85, 1158. doi:10.1103/PhysRevLett.85.1158
- Huang F. P., Kadota K., Sekiguchi T., Tashiro H., 2018, *PhRvD*, 97, 123001. doi:10.1103/PhysRevD.97.123001
- Hui L., Ostriker J. P., Tremaine S., Witten E., 2017, *PhRvD*, 95, 043541. doi:10.1103/PhysRevD.95.043541
- Irsic V., Viel M., Haehnelt M. G., Bolton J. S., Becker G. D., 2017, *PhRvL*, 119, 031302. doi:10.1103/PhysRevLett.119.031302
- Ivanytskyi O., Sagun V., Lopes I., 2020, *PhRvD*, 102, 063028. doi:10.1103/PhysRevD.102.063028
- Jiang J.-L., et al., 2019, *ApJ*, 885, 39. doi:10.3847/1538-4357/ab44b2
- Kato R., Soda J., 2020, *JCAP*, 09, 036. doi:10.1088/1475-7516/2020/09/036
- Kawai H., Oguri M., Amruth A., Broadhurst T., Lim J., 2022, *ApJ*, 925, 61. doi:10.3847/1538-4357/ac39a2
- Keung W.-Y., Marfatia D., Tseng P.-Y., 2020, *JHEP*, 2020, 181. doi:10.1007/JHEP07(2020)181
- Khlopov M. Iu., Malomed B. A., Zeldovich Ia. B., 1985, *MNRAS*, 215, 575. doi:10.1093/mnras/215.4.575
- Khmelnitsky A., Rubakov V., 2014, *JCAP*, 02, 019. doi:10.1088/1475-7516/2014/02/019
- Kulkarni M., Ostriker J. P., 2022, *MNRAS*, 510, 1425. doi:10.1093/mnras/stab3520
- Kumar A., Das H. C., Patra S. K., 2022, *MNRAS*, 513, 1820. doi:10.1093/mnras/stac1013
- Lattimer J. M., Prakash M., 2007, *Phys. Rept.*, 442, 109. doi:10.1016/j.physrep.2007.02.003
- Lee B. K. K., Chu M.-C., Lin L.-M., 2021, *ApJ*, 922, 242. doi:10.3847/1538-4357/ac2735
- Leung S.-C., et al., 2019, *ApJ*, 884, 9. doi:10.3847/1538-4357/ab3b5e
- Li A., Miao Z.-Q., Jiang J.-L., Tang S.-P., Xu R.-X., 2021, *MNRAS*, 506, 5916. doi:10.1093/mnras/stab2029
- Linares M., Shahbaz T., Casares J., 2018, *ApJ*, 859, 54. doi:10.3847/1538-4357/aabde6
- Lopes I., Panotopoulos G., 2018, *PhRvD*, 97, 024030. doi:10.1103/PhysRevD.97.024030
- Maity T. N., Queiroz F. S., 2021, *PhRvD*, 104, 083019. doi:10.1103/PhysRevD.104.083019
- Martino I. D., et al., 2017, *PhRvL*, 119, 221103. doi:10.1103/PhysRevLett.119.221103
- Menci N., et al., 2017, *ApJ*, 836, 61. doi:10.3847/1538-4357/836/1/61
- Miller M. C., et al., 2019, *ApJL*, 887, L24. doi:10.3847/2041-8213/ab50c5
- Miller, M. C., Lamb, F. K., Dittmann, A. J., et al., 2021, *ApJL*, 918, L28. doi:10.3847/2041-8213/ac089b
- Mocz P., et al., 2019, *PhRvL*, 123, 141301. doi:10.1103/PhysRevLett.123.141301
- Mukhopadhyay P., Schaffner-Bielich J., 2016, *PhRvD*, 93, 083009. doi:10.1103/PhysRevD.93.083009
- Nacir D. L., Urban F. R., 2018, *JCAP*, 10, 044. doi:10.1088/1475-7516/2018/10/044
- Nadler E. O., Gluscevic V., Boddy K. K., Wechsler R. H., 2019, *ApJL*, 878, L32. doi:10.3847/2041-8213/ab1eb2
- Nadler E. O., et al., 2021, *PhRvL*, 126, 091101. doi:10.1103/PhysRevLett.126.091101
- Niemeyer J. C., 2020, *PrPPN*, 113, 103787. doi:10.1016/j.pppn.2020.103787
- Nomura K., Ito A., Soda J., 2020, *EPJC*, 80, 419. doi:10.1140/epjc/s10052-020-7990-y
- Nori M., Murgia R., Irsic V., Baldi M., Viel M., 2019, *MNRAS*, 482, 3227. doi:10.1093/mnras/sty2888
- Ozel F., Psaltis D., 2009, *PhRvD*, 80, 103003. doi:10.1103/PhysRevD.80.103003
- Panotopoulos G., Lopes I., 2017, *PhRvD*, 96, 023002. doi:10.1103/PhysRevD.96.023002
- Panotopoulos G., Lopes I., 2017, *PhRvD*, 96, 083013. doi:10.1103/PhysRevD.96.083013
- Parkinson D., et al., 2012, *PhRvD*, 86, 103518. doi:10.1103/PhysRevD.86.103518
- Pereira J. P., et al., 2021, *ApJ*, 910, 145. doi:10.3847/1538-4357/abe633
- Pereira J. P., Beijer M., Andersson N., Gittins F., 2020, *ApJ*, 895, 28. doi:10.3847/1538-4357/ab8aca
- Perez-Garcia M. A., Silk J., Stone J. R., 2010, *PhRvL*, 105, 141101. doi:10.1103/PhysRevLett.105.141101
- Porayko N. K., Postnov K. A., 2014, *PhRvD*, 90, 062008. doi:10.1103/PhysRevD.90.062008

- Porayko N. K., et al., 2018, *PhRvD*, 98, 102002.
doi:10.1103/PhysRevD.98.102002
- Postnikov S., Prakash M., Lattimer J. M., 2010, *PhRvD*, 82, 024016. doi:10.1103/PhysRevD.82.024016
- Quddus A., et al., 2020, *J. Phys. G: Nucl. Part. Phys.*, 47, 095202. doi:10.1088/1361-6471/ab9d36
- Rafiei Karkevandi D., Shakeri S., Sagun V., Ivanytskyi O., 2022, *PhRvD*, 105, 023001.
doi:10.1103/PhysRevD.105.023001
- Riley, T. E., Watts, A. L., Bogdanov, S., et al., 2021, *ApJL*, 918, L27. doi:10.3847/2041-8213/ac0a81
- Romani, R. W., Kandel, D., Filippenko, A. V., Brink, T. G., Zheng, W., 2022, *ApJL*, 934, L17. doi:10.3847/2041-8213/ac8007
- Rogers K. K., Peiris H. V., 2021, *PhRvL*, 126, 071302.
doi:10.1103/PhysRevLett.126.071302
- Safdi B. R., Sun Z., Chen A. Y., 2019, *PhRvD*, 99, 123021.
doi:10.1103/PhysRevD.99.123021
- Sandin F., Ciarcelluti P., 2009, *Astropart. Phys.*, 32, 278.
doi:10.1016/j.astropartphys.2009.09.005
- Schive H.-Y., Chiueh T., Broadhurst T., Huang K.-W., 2016, *ApJ*, 818, 89. doi:10.3847/0004-637X/818/1/89
- Svrcek P., Witten E., 2006, *JHEP*, 06, 051.
doi:10.1088/1126-6708/2006/06/051
- Widrow L.M., Kaiser N., 1993, *ApJL*, 416, L71.
doi:10.1086/187073
- Yang S.-H., Pi C.-M., Zheng X.-P., 2021, *PhRvD*, 104, 083016. doi:10.1103/PhysRevD.104.083016
- Zheng H., Chen L.-W., 2016, *ApJ*, 831, 127.
doi:10.3847/0004-637X/831/2/127
- Zhou E.-P., Zhou X., Li A., 2018, *PhRvD*, 97, 083015.
doi:10.1103/PhysRevD.97.083015